Electronic Supplementary Material (ESI) for Chemical Communications

Natural and Magnetic Optical Activity of 2-D Chiral Cyanido-Bridged Mn^{II}-Nb^{IV} Molecular Ferrimagnets

Szymon Chorazy,[a] Robert Podgajny,*[a] Wojciech Nitek,[a] Tomasz Fic,[b] Edward Görlich,[b] Michał Rams[b] and Barbara Sieklucka[a]

[a]*Faculty of Chemistry, Jagiellonian University, Ingardena 3, 30-060 Kraków, Poland. Tel.: (4812) 6632051. E-mail: podgajny@chemia.uj.edu.pl.*
[b]*M. Smoluchowski Institute of Physics, Jagiellonian University, Reymonta 4, 30-059 Kraków, Poland.*

1. Experimental details S2
2. Photos of selected single crystals of **1**-(*S*) and **1**-(*R*) (Fig. S1) S5
3. TGA coupled with QMS analysis for **1**-(*R*) (Fig. S2) S6
4. Crystal Data and Structure Refinement for **1**-(*S*) and **1**-(*R*) (Table S1) S7
5. The crystal structure of **1**-(*S*) and **1**-(*R*): the asymmetric units with atom labelling scheme (Fig. S3) S8
6. Detailed structure parameters of **1**-(*S*) and **1**-(*R*) (Table S2) S9
7. Results of Continuous Shape Measure analysis for $[Nb^{IV}(CN)_8]^{4-}$ units in **1**-(*S*) and **1**-(*R*) (Table S3) S10
8. Ideal and observed dihedral δ and φ angles in $[Nb^{IV}(CN)_8]^{3-}$ units in **1**-(*S*) and **1**-(*R*) (Table S4) S10
9. The crystal structure of **1**-(*S*) and **1**-(*R*): the view of intrachain and interchain π-π interactions between organic ligands and the arrangement of water molecules between layers (Fig. S4) S11
10. PXRD patterns of **1**-(*R*) and **1**-(*S*) (Fig. S5) S12
11. The representative magnetic characterisation of **1**-(*R*) and **1**-(*S*) (Fig. S6) S13
12. Comment to Fig. S6 – magnetic properties of **1**-(*R*) and **1**-(*S*) S14
13. Magnetic circular dichroism spectra at various temperatures measured at H = 2 kOe for **1**-(*R*) and **1**-(*S*) (Fig. S7) S15
14. Magnetic circular dichroism spectra at various magnetic fields measured at T = 4 K for **1**-(*R*) and **1**-(*S*) (Fig. S8) S16
15. References to Supporting Information S17

1. Experimental details.

1a. Materials

$K_4[Nb^{IV}(CN)_8]\cdot 2H_2O$ was synthesized according to the published procedure.[S1] (*S*)- and (*R*)-mpm and $MnCl_2\cdot 4H_2O$ were purchased from Sigma Aldrich Co. and used without purification.

1b. Synthesis of 1-(*R*) and 1-(*S*)

1-(*R*): All operations were carried out under an Ar atmosphere. Degassed water solutions of $MnCl_2\cdot 4H_2O$ (3 mL, 10.7 mg, 0.05 mmol) and (*R*)-mpm (3 ml, 67.5 mg, 0.5 mmol) were stirred together for several minutes. Then, a degassed aqueous solution of $K_4[Nb(CN)_8]\cdot 2H_2O$ (3 mL, 12.3 mg, 0.025 mmol) was added and the resulting light orange solution was left to stand in the dark. Orange block crystals (Fig. S1a) of $\{Mn^{II}(R\text{-mpm})_2[Nb^{IV}(CN)_8]\}\cdot 4H_2O$, **1**-(*R*) appeared after a few days. Obtained material was filtrated, washed with water and dried on the air. Yield *ca.* 15 mg. The synthesis performed under an air atmosphere also gave crystals of **1**-(*R*), yet with much lower yield and with the large amount of the white amorphous by-products. IR (KBr, cm^{-1}). CN^- stretching vibrations: 2145m, 2133s, 2128vs, 2118s. Anal. Calcd. for $Mn_2Nb_1C_{36}H_{44}N_{12}O_8$: C, 44.32%; H, 4.55%; N, 17.23%. Found: C, 44.61%; H, 4.52%; N, 17.03%.

1-(*S*): The synthesis of **1**-(*S*) is the analogous to that for **1**-(*R*) with the exception of using (*S*)-mpm instead of (*R*)-mpm. Orange block crystals (Fig. S1b) of $\{Mn^{II}(S\text{-mpm})_2[Nb^{IV}(CN)_8]\}\cdot 4H_2O$, **1**-(*S*) appears after several days. Yield *ca.* 15 mg. IR (KBr, cm^{-1}). CN^- stretching vibrations: 2145m, 2133s, 2128vs, 2118s. Anal. Calcd. for $Mn_2Nb_1C_{36}H_{44}N_{12}O_8$: C, 44.32%; H, 4.55%; N, 17.23%. Found: C, 44.64%; H, 4.54%; N, 17.10%.

TGA QMS for **1**-(*R*) (Fig. S2): loss of 4 H_2O [line (*q*/*m*) 18^+], calcd. 7.4%, found 7.7%. The same results were found for **1**-(*S*) (not shown).

All syntheses analogous to that described for **1**-(*R*) or **1**-(*S*) but with using a racemic mixture of (*R*)- and (*S*)-mpm instead of enantiopure ligands were unsuccessful, and only white amorphous by-products appeared.

1c. Crystal structure determination

Single crystal diffraction data of **1**-(*R*) and **1**-(*S*) were collected on a Nonius KappaCCD diffractometer with graphite monochromated Mo Kα radiation. Cell refinement and data reduction was performed using HKL SCALEPAC and DENZO.[S2] Positions of non-hydrogen atoms were determined using SIR-97.[S3] The structure was solved by the heavy-atom Patterson method and refined by a full-matrix least-squares technique using SHELXL-97.[S4] The non-hydrogen atoms

were refined anisotropically, hydrogen atoms isotropically. Hydrogen atoms of solvent water molecules could not be located with reasonable certainty, and they are were not included in the refinement.

1d. Powder diffraction of bulk samples of 1-(*R*) and 1-(*S*)

Powder XRD patterns of **1**-(*R*) and **1**-(*S*) in the form of carefully grinded powder sealed in 0.7 mm glass capillaries were measured on a PANalytical X'Pert PRO MPD diffractometer with a capillary spinning add-on using CuKα radiation (λ = 1.54187 Å). The patterns were collected at room temperature in the 4 - 50° 2θ range. The reference powder patterns of **1**-(*R*) and **1**-(*S*) coming from single-crystal XRD models were generated using Mercury 3.0 software.

The experimental XRD patterns of **1**-(*R*) and **1**-(*S*) fit well the patterns calculated from single-crystal XRD experiment (Fig. S5) which proves the purity of bulk samples used in the measurements of magnetic and optical properties.

1e. Physical techniques

Infrared spectra were measured in KBr pellets between 4000 and 400 cm^{-1} using a Bruker EQUINOX 55 FT-IR spectrometer. Elemental analyses of C, H, N were performed using EuroEA EuroVector elemental analyzer. Thermogravimetric data in the temperature range 25–400 °C were collected on a Mettler Toledo TGA/SDTA 851^e microthermogravimeter equipped with QMS Thermostar GSD 300 T Balzers at a heating rate of 10 °C/min in Ar atmosphere using positive ionisation. The UV-Vis absorption spectra both for aqueous solution of (*R*)-mpm as well as for the powder samples of **1**-(*R*) and $K_4[Nb(CN)_8]$ mixed with $BaSO_4$ were measured by a Perkin Elmer Lambda 35 spectrophotometer. NCD spectra were collected on the powder samples in KBr pellets using JASCO J-810 spectropolarimeter.

Magnetic measurements were performed using Quantum Design MPMS-XL. The magnetic data were collected for dry powder samples, and were corrected for the diamagnetic contribution using Pascal constants.[S5]

MCD spectra were measured using a JASCO J-810 spectropolarimeter equipped with an Oxford Instruments cryostat Spectromag SM 4000-9T with a split-coil superconducting magnet. The powder samples of **1**-(*R*) and **1**-(*S*) were measured in KBr pellets placed in a copper sample holder that was screwed to the lower end of the sample probe. The cryostat windows and the sample holder were checked before measurements, and they did not contribute to the MCD signals. Magnetic field was applied in the direction parallel to the polarised laser beam. Data was collected with the help of JASCO spectra manager software. The measured signal was the sum of NCD and MCD spectra,

and the final MCD spectra were obtained by subtraction of NCD part (NCD contribution could be estimated as the signal measured at T = 100 K and H = 2 kOe where no significant MCD part was detected, Fig. S5 and S6).

1f. Calculations

Continuous Shape Measure Analysis for coordination spheres of eight-coordinated $[Nb^{IV}(CN)_8]^{4-}$ ions was performed by SHAPE software ver. 1.1b.[S6-S8]

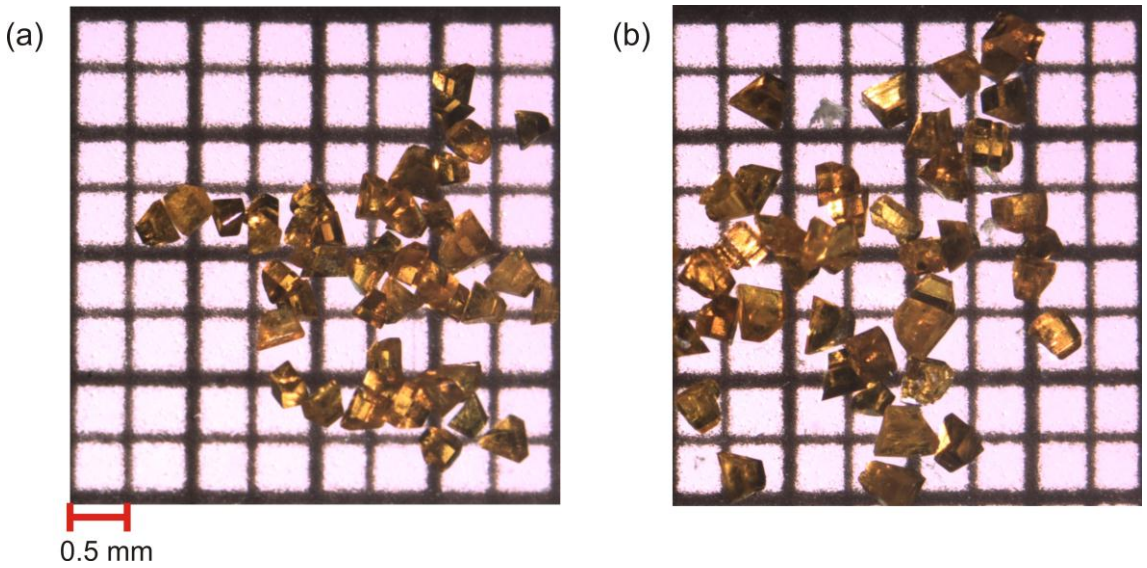

Fig. S1 Photos of selected single crystals of **1**-(*S*) (a) and **1**-(*R*) (b). Note completely the same shape and colour for both enantiomorphs.

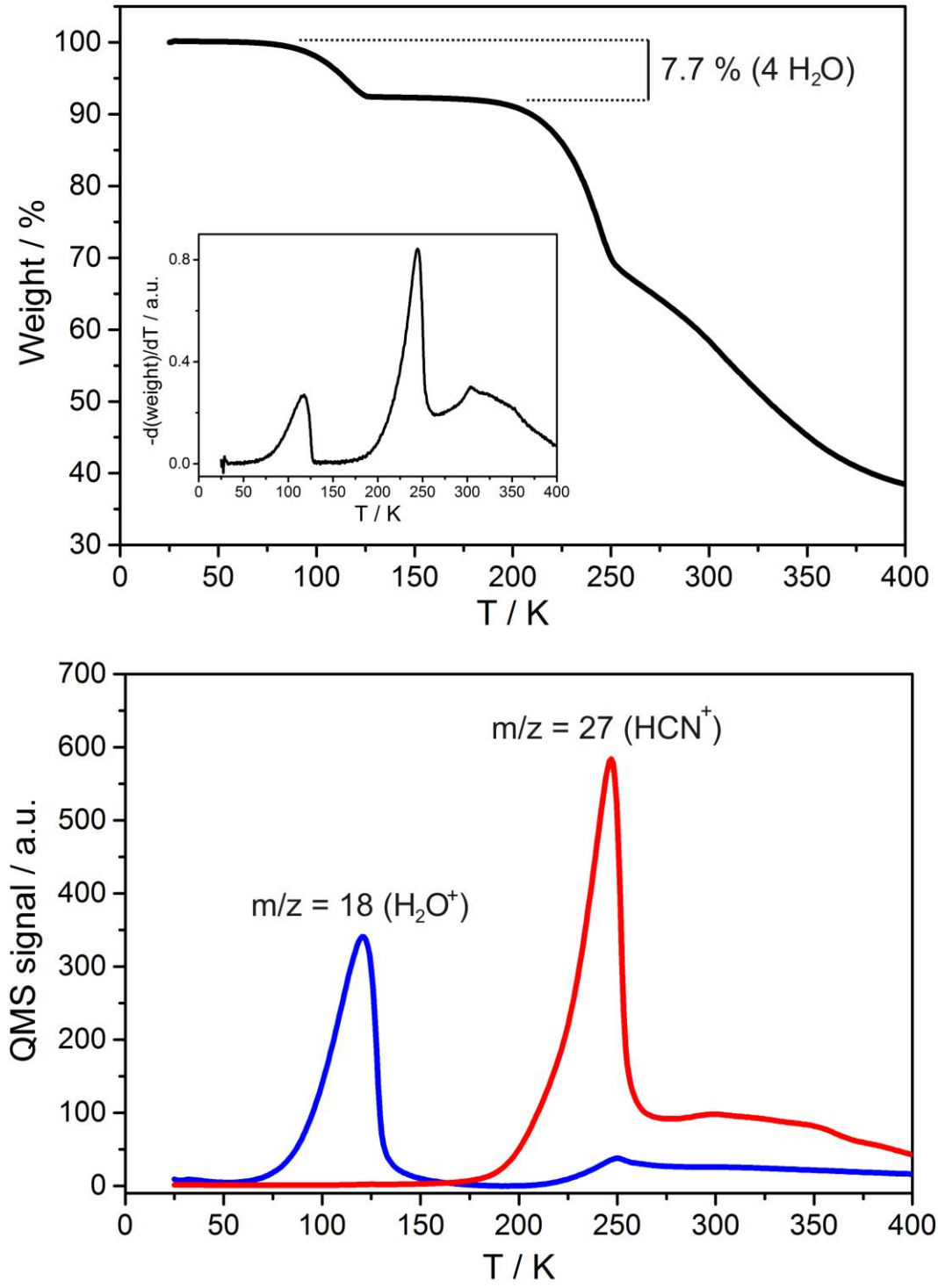

Fig. S2 TGA curve (top) and its first derivative curve (the inset, top) coupled with QMS analysis (bottom) for **1**-(*R*). The first step around 110 °C corresponds to the loss of four water molecules (weight loss of 7.7 %, QMS peak with m/z = 18 related to H_2O^+). The second step around 230 °C corresponds to the removal of cyanides (weight loss more than 20 %, QMS peak with m/z = 27 related to HCN^+). The same results were found for **1**-(*S*) (not shown).

Table S1 Crystal Data and Structure Refinement for **1**-(*R*) and **1**-(*S*)

compound		**1**-(*S*)	**1**-(*R*)
method		single-crystal XRD	single-crystal XRD
formula		$Mn_2Nb_1C_{36}H_{44}N_{12}O_8$	$Mn_2Nb_1C_{36}H_{44}N_{12}O_8$
formula weight [g·mol^{-1}]		975.62	975.62
T [K]		293(2)	293(2)
λ [Å]		0.71069 (Mo Kα)	0.71073 (Mo Kα)
crystal system		monoclinic	monoclinic
space group		$P2_1$	$P2_1$
unit cell	***a* [Å]**	12.950(5)	12.946(2)
	***b* [Å]**	13.276(5)	13.280(2)
	***c* [Å]**	13.810(5)	13.803(2)
	β [deg]	112.258(5)	112.237(2)
V [Å^3]		2197.4(14)	2196.6(6)
Z		2	2
calculated density [g·cm^{-3}]		1.475	1.475
absorption coefficient [cm^{-1}]		0.883	0.883
F(000)		974	974
crystal size [mm x mm x mm]		0.16 × 0.14 × 0.13	0.20 × 0.17 × 0.13
Θ range [deg]		1.59 – 27.48	1.59 – 27.48
limiting indices		-16 < h < 16 -17 < k < 17 -17 < l < 17	-16 < h < 16 -17 < k < 17 -17 < l < 17
collected reflections		57363	18511
unique reflections		10047	10029
R_{int}		0.0522	0.0189
completeness [%]		100	100
refinement method		full-matrix least-squares on F^2	full-matrix least-squares on F^2
data/restraints/parameters		10047/1/537	10029/1/537
Flack parameter		-0.022(13)	-0.008(15)
GOF on F^2		1.047	1.176
final *R* indices		R_1 = 0.0313 [$I > 2\sigma(I)$] wR_2 = 0.0792 (all data)	R_1 = 0.0350 [$I > 2\sigma(I)$] wR_2 = 0.1012 (all data)
largest diff peak and hole		0.663 and -0.651 e·A^{-3}	1.084 and -0.571 e·A^{-3}

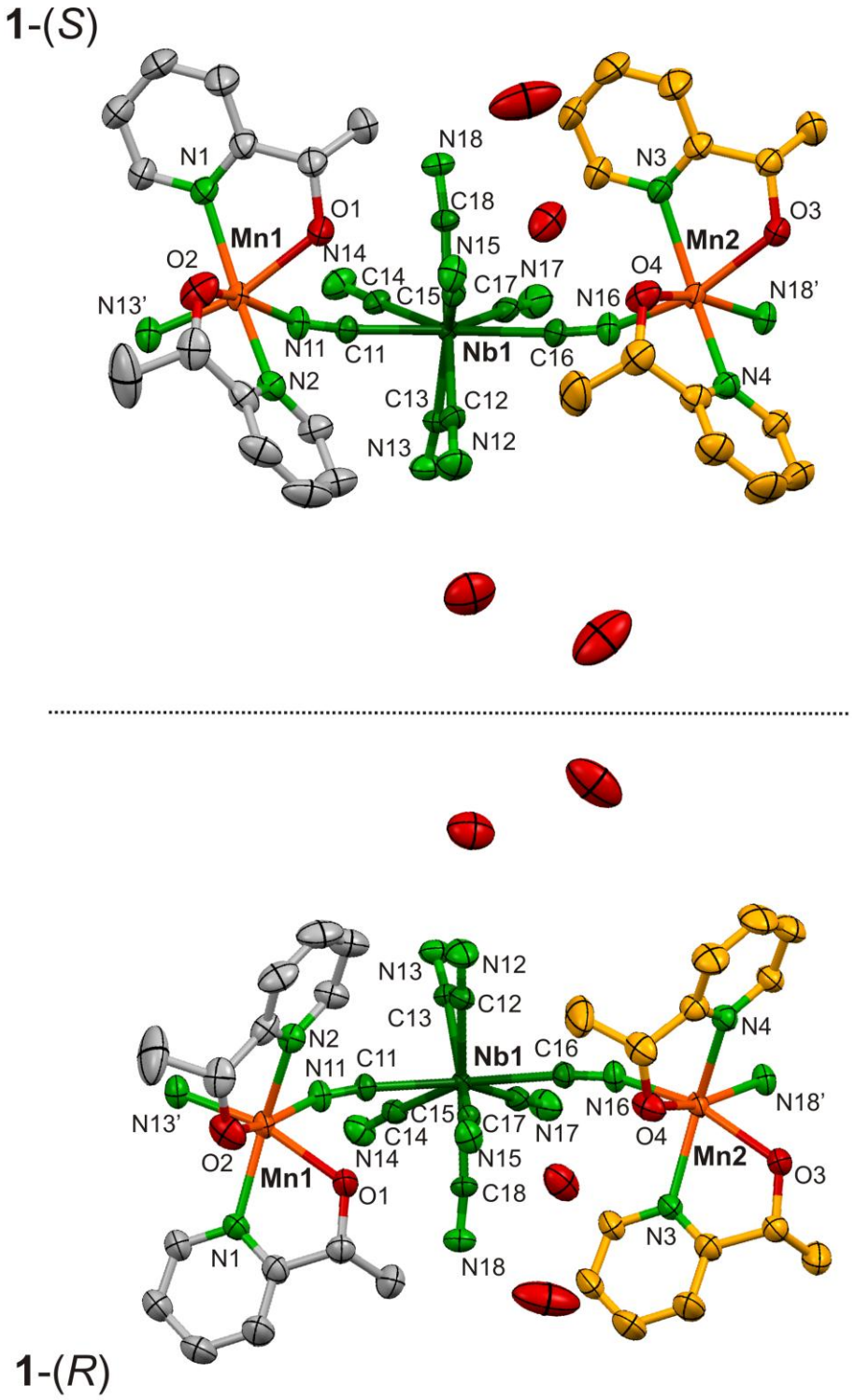

Fig. S3 The crystal structure of **1**-(*S*) (top) and **1**-(*R*) (bottom): the asymmetric units with atom labelling scheme. Atom spheres are shown with 50% probability ellipsoids. Hydrogen atoms are omitted for clarity. Colours: Mn – orange, Nb – dark green, O – red, N – light green, C (cyanides) – green, C (organic ligand coordinated to Mn1) – grey, C (organic ligand coordinated to Mn2) – yellow.

Table S2 Detailed structure parameters of **1**-(*S*) and **1**-(*R*)

Parameter	**1**-(*S*)	**1**-(*R*)
Nb1-C	2.244(5) – 2.275(6) Å	2.239(7) – 2.269(6) Å
C-N (Nb1)	1.116(8) – 1.186(8) Å	1.137(10) – 1.190(10) Å
Nb1-C-N	170.5(5) – 177.9(6)°	170.7(6) – 176.9(8)°
Mn1-N-C	154.9(4)° (N11-C11) 158.9(5)° (N13-C13)	154.8(6)° (N11-C11) 159.5(7)° (N13-C13)
Mn2-N-C	155.2(4)° (N18-C18) 160.4(5)° (N16-C16)	157.0(6)° (N18-C18) 160.3(6)° (N16-C16)
Mn1-N(CN)	2.165(5) Å (N13); 2.183(5) Å (N11)	2.161(7) Å (N13); 2.183(7) Å (N11)
Mn2-N(CN)	2.179(5) Å (N16); 2.183(5) Å (N18)	2.178(7) Å (N11); 2.180(7) Å (N18)
Mn1-N(py)	2.258(5) Å (N2); 2.271(5) Å (N1)	2.261(7) Å (N2); 2.276(7) Å (N1)
Mn2-N(py)	2.268(5) Å (N3); 2.284(5) Å (N4)	2.271(7) Å (N3); 2.292(7) Å (N4)
Mn1-O	2.197(5) Å (O2); 2.245(5) Å (O1)	2.199(6) Å (O2); 2.248(6) Å (O1)
Mn2-O	2.216(5) Å (O4); 2.290(4) Å (O3)	2.225(6) Å (O4); 2.296(6) Å (O3)
N(CN)-Mn1-N(CN)	95.10(19)°	95.3(3)°
N(CN)-Mn2-N(CN)	96.26(19)°	96.7(3)°
N(py)-Mn1-O	70.8(2)° (N1,O1); 70.8(2)° (N2,O2) 83.5(2)° (N1,O2); 96.3(2)° (N2,O1)	70.2(2)° (N1,O1); 70.3(3)° (N2,O2) 83.5(3)° (N1,O2); 96.6(2)° (N2,O1)
N(py)-Mn2-O	71.2(2)° (N4, O4); 71.7(2)° (N3, O3) 93.6(2)° (N4, O3); 81.3(2)° (N3, O4)	70.8(2)° (N4,O4); 72.0(2)° (N3,O3) 93.8(2)° (N4,O3); 81.4(2)° (N3,O4)
N(py)-Mn1-N(CN)	94.6(2)° (N13, N1) 112.39(19)° (N11, N1) 98.8(2)° (N13, N2) 91.2(2)° (N11, N2)	94.3(3)° (N13, N1) 112.7(3)° (N11, N1) 99.2(3)° (N13, N2) 91.4(3)° (N11, N2)
N(py)-Mn2-N(CN)	93.0(2)° (N16, N3) 114.76(19)° (N18, N3) 103.75(19)° (N16, N4) 90.20(19)° (N18, N4)	93.0(3)° (N16, N3) 114.9(3)° (N18, N3) 103.2(3)° (N16, N4) 90.3(2)° (N18, N4)
O-Mn1-N(CN)	86.78(18)° (N11, O1) 164.8(2)° (N13, O1) 160.56(19)° (N11, O2) 94.7(2)° (N13, O2)	87.2(2)° (N11, O1) 163.9(3)° (N13, O1) 160.8(3)° (N11, O2) 93.7(3)° (N13, O2)
O-Mn2-N(CN)	83.47(17)° (N18, O3) 162.68(18)° (N16, O3) 160.75(19)° (N18, O4) 93.2(2)° (N16, O4)	82.9(2)° (N18, O3) 163.0(2)° (N16, O3) 160.3(2)° (N18, O4) 93.2(3)° (N16, O4)
O-Mn1-O	88.2(2)°	88.9(3)°
O-Mn2-O	92.42(19)°	92.5(3)°
N(py)-Mn1-N(py)	151.72(19)°	151.1(3)°
N(py)-Mn2-N(py)	148.35(19)°	148.3(3)°

Table S3 Results of Continuous Shape Measure analysis for $[Nb^{IV}(CN)_8]^{4-}$ units in **1**-(*S*) and **1**-(*R*)

$[Nb1(CN)_8]^{4-}$	**1**-(*S*)	**1**-(*R*)
CSM BTP-8[§]	1.733	1.740
CSM SAPR-8	2.800	2.808
CSM DD-8	0.344	0.345

[§]CSM BTP-8 – the parameter corresponding to the biccapped trigonal prism;
CSM SAPR-8 – the parameter corresponding to the square antiprism;
CSM DD-8 – the parameter corresponding to the dodecahedron;
CSM = 0 for the ideal geometry and increases with the degree of distortion.[S6-S8]

Table S4 Ideal and observed dihedral δ and φ angles in $[Nb^{IV}(CN)_8]^{4-}$ units in **1**-(*S*) and **1**-(*R*)[S9]

Complex	δ [deg]	φ [deg]
Ideal BTP-8	0; 21.8; 48.2; 48.2	14.1
Ideal SAPR-8	0; 0; 52.4; 52.4	24.5
Ideal DD-8	29.5; 29.5; 29.5; 29.5	0
$[Nb1(CN)_8]^{3-}$ in **1**-(*S*)	24.3; 30.1; 34.7; 36.0	3.7
$[Nb1(CN)_8]^{3-}$ in **1**-(*R*)	23.7; 30.2; 34.9; 35.6	3.7

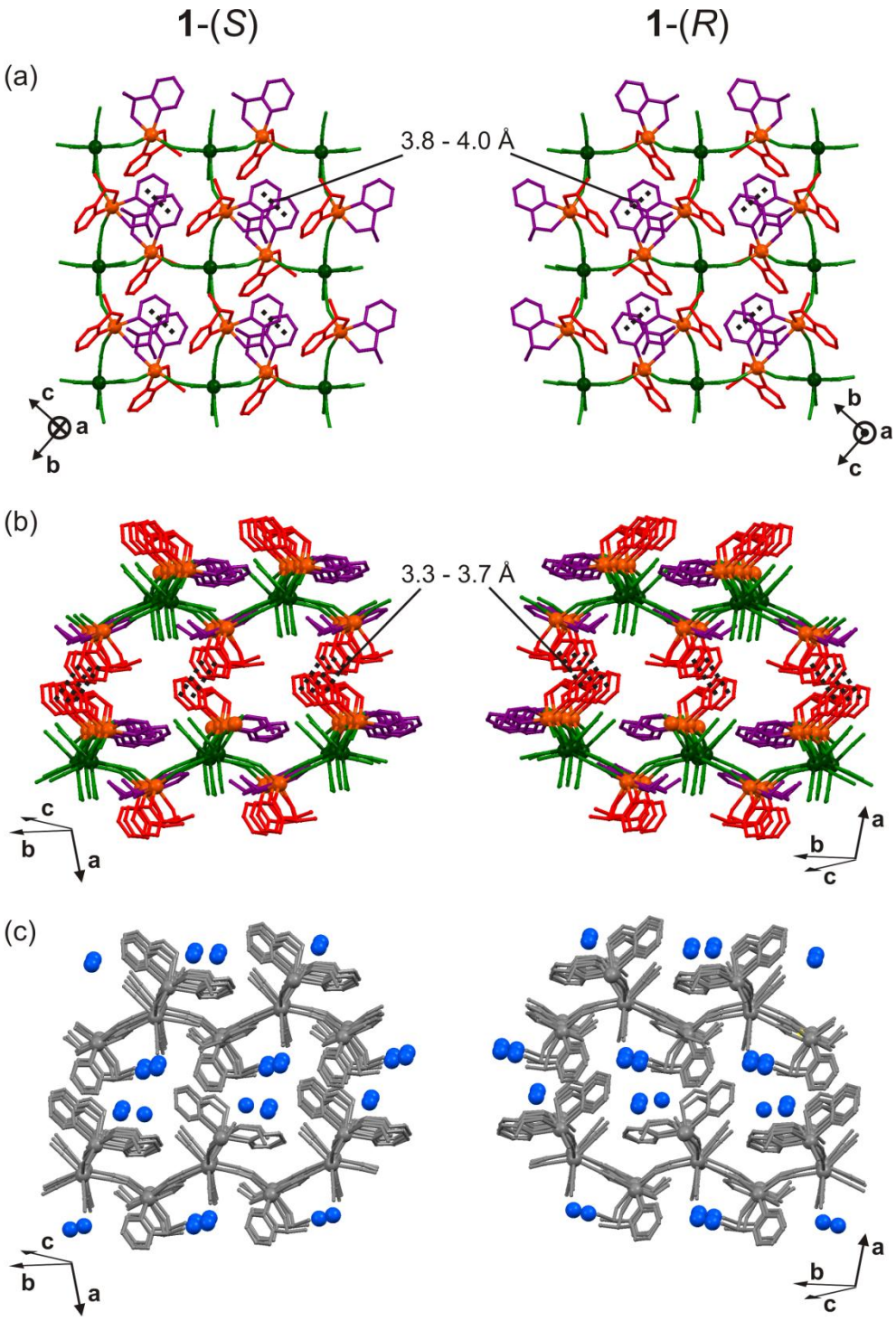

Fig. S4 The crystal structure of **1**-(*S*) (left panel) and **1**-(*R*) (right panel): the view of coordination layers in bc plane with the marking of intrachain π-π interactions between aromatic rings of (*S*)- and (*R*)-mpm ligands (a), the view of the closest interchain contacts stabilized by π-π interactions (b), the arrangement of solvent water in the space between layers (c). Hydrogen atoms are omitted for clarity. Colours in (a) and (b): Eu – orange; W, CN^- – green; C, N, O (organic ligand) – red or purple. Colours in (c): atoms of coordination skeleton – grey, O (water) – blue.

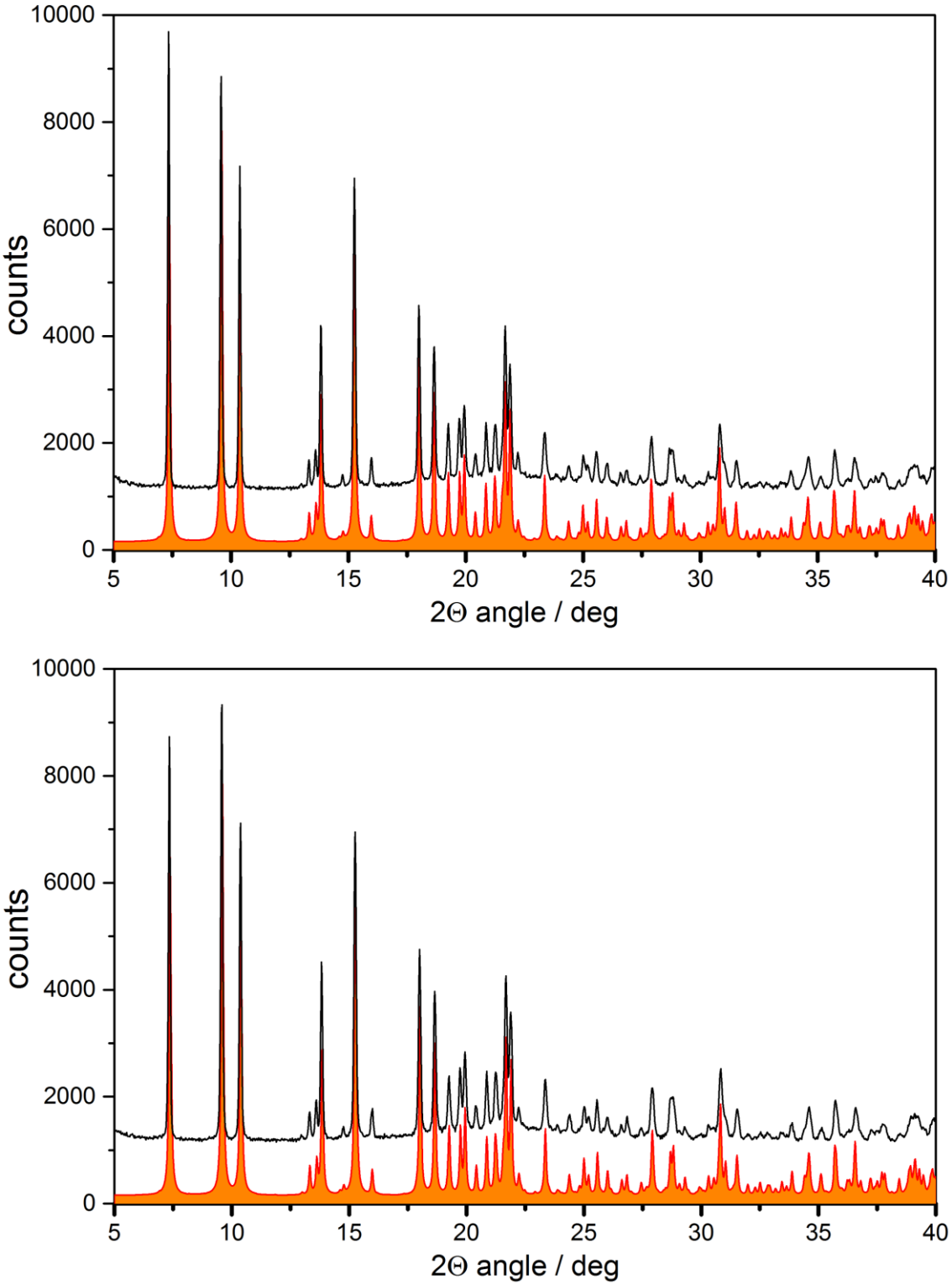

Fig. S5 PXRD patterns of compounds **1**-(*S*) (top) and **1**-(*R*) (bottom). Black solid lines are the experimental patterns and colour lines are the respective calculated patterns from single-crystal XRD models.

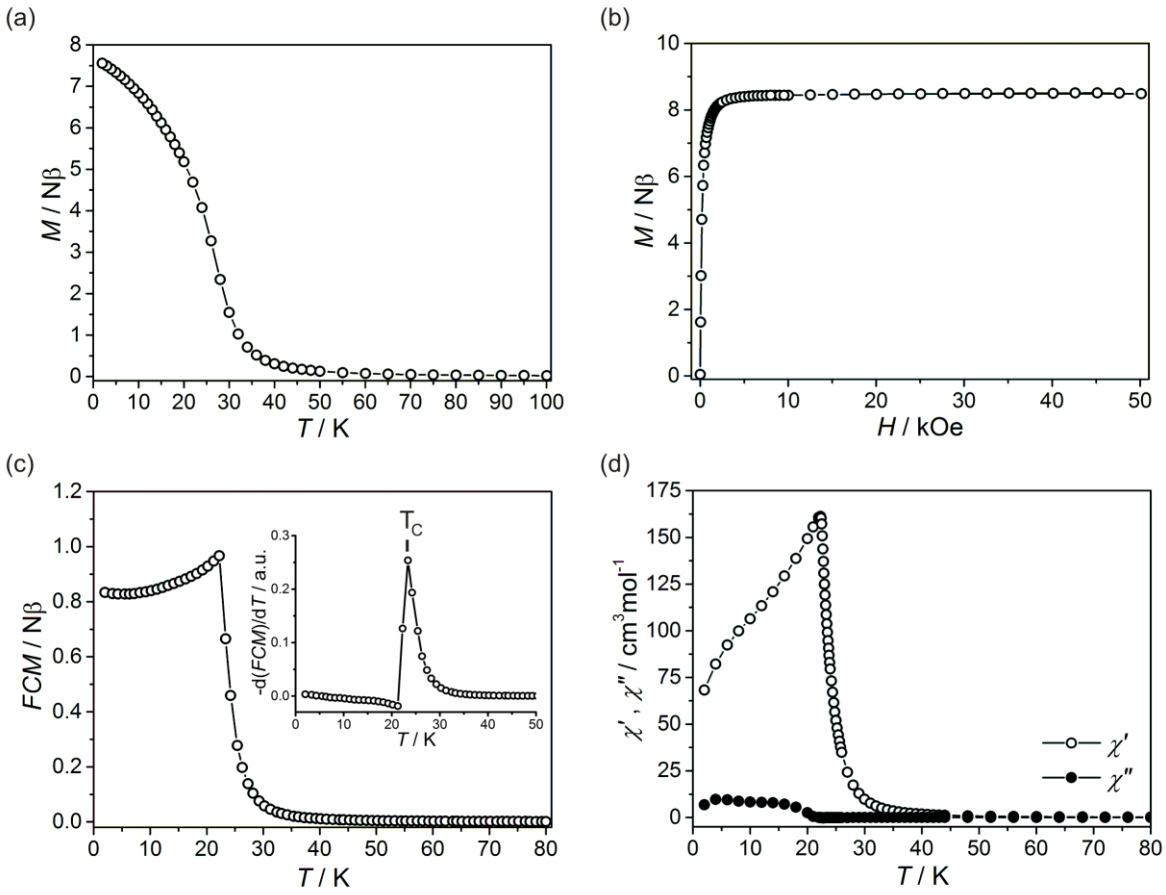

Fig. S6 The representative magnetic characterisation of **1**-(*R*): (a) temperature dependence of magnetization for H = 1 kOe, (b) field-dependence of magnetization at T = 2 K, (c) field-cooled magnetization for H = 20 Oe together with the temperature dependence of its first derivative (the inset), and (d) *ac* magnetic characteristics (H_{dc} = 0 Oe, H_{ac} = 3Oe). Identical characteristics were observed for **1**-(*S*) (not shown).

Comment to Figure S6 – magnetic properties of 1-(*R*) and 1-(*S*)

The temperature dependence of the magnetization measured at 1 kOe for **1**-(*R*) is presented in Fig. S6a. The room temperature $\chi_M T$ value of 8.5 $cm^3mol^{-1}K$ for $Mn^{II}_2Nb^{IV}$ unit is very close to 9.1 $cm^3mol^{-1}K$ expected for two high-spin Mn^{II} (S = 5/2, g = 2.0) and one Nb^{IV} (S = 1/2, g = 2.0). On cooling, M value increases firstly slowly, and later, below 40 K, increases abruptly reaching the high value of 7.6 Nβ at 2 K suggesting the presence of long-range magnetic ordering. The magnetization versus applied magnetic field curve measured at 2 K (Fig. S6b) shows fast increase of magnetization. The saturation magnetization of 8.6 Nβ is close to 9 Nβ corresponding to magnetic structure with one Nb^{IV} aligned antiparallel to two Mn^{II}. This strongly indicates that **1**-(*R*) reveals cyano-mediated antiferromagnetic Mn^{II}-Nb^{IV} antiferromagnetic coupling leading to the long-range ordering of a ferrimagnetic character which is with a good agreement with other known cyanido-bridged Mn^{II}-Nb^{IV} magnetic networks.[S10] No magnetic hysteresis is observed at 2 K indicating the soft character of this molecular ferrimagnet. The critical temperature of 23.5 K for this ferrimagnet was estimated from the first derivative of the field-cooled magnetization measured at small applied field of 20 Oe (Fig. S6c). This value is also consistent with the *ac* magnetic data showing the anomaly characteristic for the phase transition to the magnetically ordered phase at this temperature (Fig. S6d). Identical magnetic characteristics were observed for **1**-(*S*) (not shown).

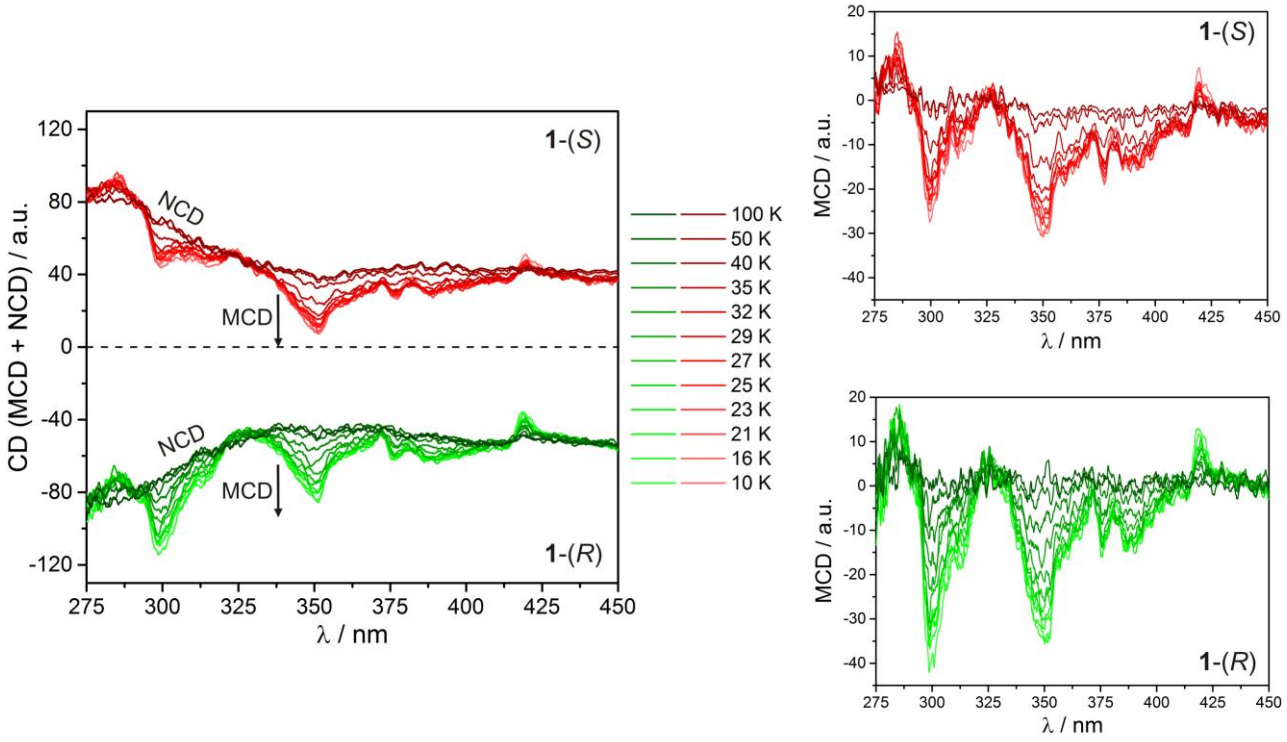

Fig. S7 MCD spectra at various temperatures collected at H = 2 kOe for **1**-(*R*) and **1**-(*S*): (left side) total CD spectra (NCD together with MCD signal) for both enantiomers, and (right side) MCD spectra after the subtraction of NCD contribution for **1**-(*S*) (top) and **1**-(*R*) (bottom). Red lines correspond to the signal for **1**-(*S*) when green lines are related to **1**-(*R*).

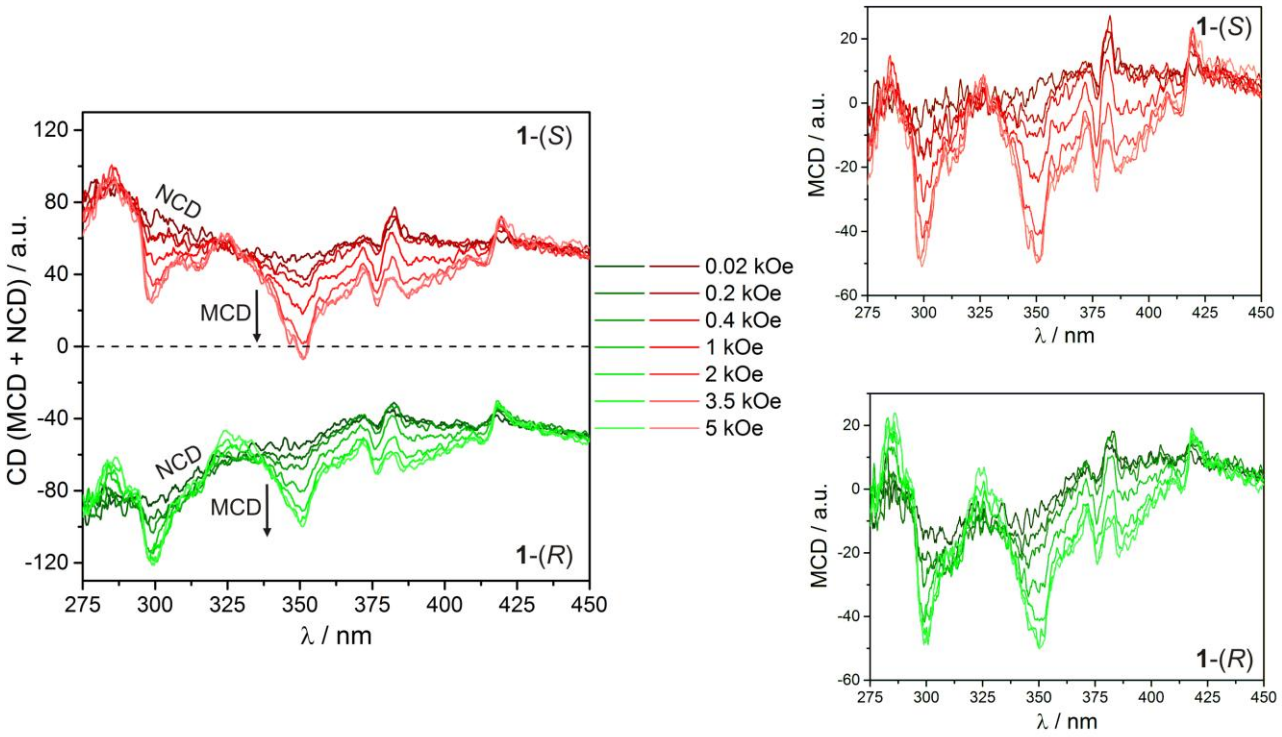

Fig. S8 MCD spectra at various magnetic fields collected at T = 4 K for **1**-(*R*) and **1**-(*S*): (left side) total CD spectra (NCD together with MCD signal) for both enantiomers, and (right side) MCD spectra after the subtraction of NCD contribution for **1**-(*S*) (top) and **1**-(*R*) (bottom). Red lines correspond to the signal for **1**-(*S*) when green lines are related to **1**-(*R*).

References to Supporting Information

(S1) P. M. Kiernan and W. P. Griffith, *J. Chem. Soc., Dalton Trans*., 1975, 2489.

(S2) Z. Otwinowski and W. Minor, *Methods in Enzymology*, Vol. 276, *Macromolecular Crystallography*, *Part A*, edited by C. W. Carter Jr and R. M. Sweet, Academic Press, New York, 1997, pp. 307-326.

(S3) A. Altomare, M. C. Burla, M. Camalli, G. L. Cascarano, C. Giacovazzo, A. Guagliardi, A. G. G. Moliterni, G. Polidori and R. Spagna, *J. Appl. Cryst.*, 1999, **32**, 115.

(S4) G. M. Sheldrick, *Acta Cryst.* 2008, **A64**, 112-122.

(S5) G. A. Bain and J. F. Berry, *J. Chem. Edu*., 2008, **85**, 532.

(S6) M. Llunell, D. Casanova, J. Cirera, J. Bofill, P. Alemany, S. Alvarez, M. Pinsky and D. Avnir, *SHAPE v. 1.1b Program for the Calculation of Continuous Shape Measures of Polygonal and Polyhedral Molecular Fragments*, University of Barcelona: Barcelona, Spain, 2005.

(S7) D. Casanova, J. Cirera, M. Llunell, P. Alemany, D. Avnir and S. Alvarez, *J. Am. Chem. Soc*., 2004, **126**, 1755.

(S8) S. Alvarez, P. Alemany, D. Casanova, J. Cirera, M. Llunell and D. Avnir, *Coord. Chem. Rev.*, 2005, **249**, 1693.

(S9) E. L. Muetterties and L. J. Guggenberger, *J. Am. Chem. Soc*., 1974, **96**, 1748.

(S10) B. Nowicka, T. Korzeniak, O. Stefańczyk, D. Pinkowicz, S. Chorazy, R. Podgajny and B. Sieklucka, *Coord. Chem. Rev.*, 2012, **256**, 1946.